Automated segmentation of psoas major muscle in X-ray CT images by use of a shape model: preliminary study

Naoki Kamiya · Xiangrong Zhou · Huayue Chen · Chisako Muramatsu ·
Takeshi Hara · Ryujiro Yokoyama · Masayuki Kanematsu · Hiroaki Hoshi ·
Hiroshi Fujita

Abstract Our motivation was to provide an automatic tool for radiologists and orthopedic surgeons for improving the quality of life of an aging population. We propose a method for generating a shape model and a fully automated segmenting scheme for the psoas major muscle in X-ray CT images by using the shape model. Our approach consists of two steps: (1) The generation of a shape model and its application to muscle segmentation. The shape model describes the muscle's outer shape and has two parameters, an outer shape parameter and a fitting parameter. The former was determined by approximating of the outer shape of the muscle region in training cases. The latter was determined for each test case in the recognition process. (2) Finally, the psoas major muscle was segmented by use of the shape model. To evaluate the performance of the method, we applied it to CT images for constructing the shape models by using 20 cases as training samples; 80 cases were used for testing. The accuracy of this method was measured by comparison of the extracted muscle regions with regions that were identified manually by an expert radiologist. The experimental results of the segmentation of the psoas major muscle gave a mean Jaccard similarity coefficient of 72.3%. The mean true segmentation coefficient was 76.2%. The proposed method can be

N. Kamiya (✉) · X. Zhou · C. Muramatsu · T. Hara · H. Fujita
Division of Regeneration and Advanced Medical Sciences,
Department of Intelligent Image Information,
Graduate School of Medicine, Gifu University,
Yanagido 1-1, Gifu 501-1194, Japan
e-mail: kamiya@fjt.info.gifu-u.ac.jp

X. Zhou
e-mail: zxr@fjt.info.gifu-u.ac.jp

C. Muramatsu
e-mail: chisa@fjt.info.gifu-u.ac.jp

T. Hara
e-mail: hara@fjt.info.gifu-u.ac.jp

H. Fujita
e-mail: fujita@fjt.info.gifu-u.ac.jp

N. Kamiya
Department of Information and Computer Engineering, Toyota
National College of Technology, 2-1 Eiseicho, Toyota, Aichi
471-8525, Japan

H. Chen
Department of Anatomy, Graduate School of Medicine,
Gifu University, Gifu 501-1194, Japan
e-mail: huayue@gifu-u.ac.jp

R. Yokoyama · M. Kanematsu
Department of Radiology Services, Gifu University Hospital,
Gifu 501-1194, Japan
e-mail: ryujiro@cc.gifu-u.ac.jp

M. Kanematsu
e-mail: masa-gif@umin.net

M. Kanematsu
Department of Radiology, Gifu University School of Medicine
and Gifu University Hospital, Gifu 501-1194, Japan

H. Hoshi
Division of Tumor Control, Department of Radiology,
Graduate School of Medicine, Gifu University,
Gifu 501-1194, Japan
e-mail: hoshi@cc.gifu-u.ac.jp

used for the analysis of cross-sectional area and muscular thickness in a transverse section, offering radiologists an alternative to manual measurement for saving their time and improving the reproducibility of segmentation.

1 Introduction

Recognition of the skeletal muscles in the abdominal region is very important for health care. These muscles are classified into two categories: surface muscles and deep muscles. Because the deep muscles cannot be examined by touch, electronic signal processing and imaging techniques are used for diagnosing the deep-muscle region. The psoas major is a deep muscle that plays a major role in walking. It is particularly important to analyze this muscle because of the age-related hypokinesia that becomes manifest with changes in this muscle region. For example, in Japan, there are increasing incidences of elderly people becoming physically handicapped after suffering a fall. Sixty-two percent of these falls result in physical damage, of which 12% result in bone fractures and 8% in the victims "requiring constant help and care" [1]. Furthermore, a decrease in muscle volume is one of the factors in falls suffered by the elderly [2].

For maintaining the quality of life of the elderly, muscle volume measurement as a component of health care for the aged is a critical task [2].

Various factors influence the falls suffered by the elderly. It is considered that elderly people fall because of their weak lower-extremity muscles. Atrophy of the psoas major, in particular, affects the walking and exercising ability of elderly people, according to a reported study in which the cross-sectional area (CSA) of the psoas major was determined [3]. The function of this muscle can be maintained by daily exercise. It has also been reported that the decrease in the CSA of the psoas major is greatest in people in their 70s and older [3]. Therefore, it is necessary to protect this muscle from age-related damage. To do so, it is necessary to measure this muscle region quantitatively. The automated segmentation of the muscle by computer, instead of manual measurement by a doctor, can relieve doctors' heavy workload, save diagnostic time, and improve the reproducibility of segmentation.

It has recently become possible to obtain high-definition CT images quickly; however, the number of images increases to as many as a thousand slices per patient. CT images showing skeletal muscles are of little use to doctors because their interest lies in the internal organs that are affected by disease. Therefore, effective use of image information is expected for CT images of the torso, which were obtained not for the diagnosis of muscles, but for other purposes (e.g., a diseased organ). Because all torso CT slices contain muscle regions, we propose an effective use of these images. In our proposed method, our goal is to segment and analyze the muscle region in non-contrast CT images.

The goal of previous research in the recognition of skeletal muscles in medical images was to develop an anatomic database or to assist doctors in surgery. A systematic organ visualization method was proposed in the Visible Human Project [4, 5] for CT images. This method could be used for identifying some muscles, commencing from the psoas major muscle, which were segmented manually. A modeling method for muscles in the crural area was then proposed for analysis of their motor function in MR images [6]. A recognition method for the temporal muscle was proposed for surgical planning and analysis of loss of the mastication function [7]. These two methods, however, were used for MR images. It remains a question whether they can be applied to CT images in which the boundaries between skeletal muscle and organ regions are unclear. In the analysis of the density histogram of the CT images, the overlapping of the pixel values of the organ region and the skeletal muscle region makes it difficult to identify the boundaries between the skeletal muscles and other tissues by use of a density histogram only.

To accomplish the segmentation of the muscle, we have been developing a computer-aided diagnosis (CAD) system for the skeletal muscles in the torso region and have obtained some positive results in the automated recognition of the skeletal muscles in the chest and abdominal regions [8–10]. However, a recognition method which considers the anatomic shape of the muscles has not yet been realized.

In this paper, we propose a novel method for automatically segmenting the psoas major muscle by means of a shape model with a mathematical function. We applied this model in the muscle recognition process for test cases. Finally, we evaluated the accuracy of the CSA and the volume obtained by the proposed method in comparison with the muscle region segmented manually by an anatomy expert in terms of the Jaccard similarity coefficient (JSC) [11] and the true segmentation coefficient (TSC) [12]. In addition, we compared the segmentation time required for manual, semi-automatic, and fully automatic segmentation in terms of time reduction. We were able to show not only that skeletal muscle recognition in a CT image was possible, an achievement that a past study considered difficult, but also that this method could be applied to images obtained by other imaging modalities because it is based on anatomic information, as in MRI, for example.

2 Materials and methods

2.1 Materials

This method was applied to one hundred data sets of X-ray CT images that were generated by a GE scanner (Light-Speed) with a slice interval of 0.625 mm and a voxel spacing of 0.625 mm × 0.625 mm. Twenty data sets were used for training of the system by generating the shape model, and the other 80 data sets were employed for validation purposes. In our previous project [8–10], our approach was to generate normal organ models, which we would employ to recognize abnormal cases that did not fit the model well. In this study, therefore, we used cases with no illness in the psoas major muscle for generating the shape model. The absence of illness in the psoas major muscle was judged by a radiologist with other clinical findings and interpretation of CT. We selected the training cases, which were used for the model generation by using a stratified randomization method [13] for men and women in five age groups from the 40s to 80s. Our purpose in this study was to validate the segmentation accuracy; therefore, the test cases were randomly selected from the normal cases and consisted of 42 males (43–83 years old; mean, 65.5; median, 71) and 38 females (46–80 years old; mean, 60.7; median, 58). This study was approved by our institutional review board (IRB).

2.2 Overview of the method

An overview of our proposed method is shown in Fig. 1a. The original CT images become the input images. The segmented skeletal images generated from the original CT images also become input images. These segmented skeletal images are generated by a method based on skeletal connectivity [8]. First, the approximate skeletal region is segmented by means of density-based methods such as gray-level thresholding. Next, each precise skeletal region is recognized sequentially on the basis of implicit anatomic knowledge of its pattern of connection, shape, and spatial relationships. The key steps in our proposed method are: (a) generation of CT images, (b) shape model generation

for the psoas major muscle, (c) application of the shape model in the recognition process, and (d) automatic extraction of the region of the psoas major muscle.

Our proposed model is based on the definition of anatomic location, direction, and shape. In the model-generating process (Fig. 1b), the anatomic shapes of the muscle models are simplified by use of five approximate functions. The muscle recognition (Fig. 1c) makes it possible to find the best region of muscle in the segmentation process (Fig. 1d) using the shape model (Fig. 1b) that is provided by the input volume (Fig. 1a), referred to as vol. The region of the muscle is determined by three parameters, i.e., p, θ, and s, which correspond to the location, orientation, and shape features, respectively, of the muscles. By use of a conditional probability $\Pr(p, \theta, s \mid \text{vol})$, the proposed method can be formulated as

$$(\hat{p}, \hat{\theta}, \hat{s}) = \arg\max_{p,\theta,s} \Pr(p, \theta, s \mid \text{vol}). \tag{1}$$

Solving Eq. 1 involves estimation of the three parameters, p, θ, and s, which are defined individually in 3D space. As a result, the determination of these parameters requires computation in 9D space, which is too expensive for practical purposes. In our approach, therefore, the 9D parameter space is decomposed into three marginal spaces as follows:

$$\Pr(p, \theta, s \mid \text{vol}) = \Pr(p \mid \text{vol}) \Pr(\theta \mid p, \text{vol}) \Pr(s \mid \theta, p, \text{vol}). \tag{2}$$

The solution to the $\Pr(p \mid \text{vol})$, $\Pr(\theta \mid p, \text{vol})$, and $\Pr(s \mid \theta, p, \text{vol})$ in Eq. 2 is described in Sects. 2.4.1, 2.4.2, and 2.4.3, respectively. First, the spatial location of the muscle is determined by the term $\Pr(p \mid \text{vol})$. The anatomic feature point p represents a set of landmarks (LMs) which are determined from the segmented skeletal images. Next, the muscle orientation is defined by the term $\Pr(\theta \mid p, \text{vol})$, where the muscle direction θ is determined based on the anatomic centerline connecting the two LMs, corresponding to the origin and the insertion of the muscle. $\Pr(p \mid \text{vol})$ and $\Pr(\theta \mid p, \text{vol})$ become 1 if the LMs are accurately set based on the anatomic definition; otherwise, they are zero. Finally, the shape feature s is determined following the model-building process. The shape feature s consists of two sub-parameters, α and β; the shape parameter α is determined by use of the training database, and the fitting parameter β is determined dynamically for a test case in the recognition process. Finally, the muscle region (i.e., $\Pr(s \mid \theta, p, \text{vol})$, see Eq. 2) is determined.

The shape model-building process (manually inputting p and θ, and also determining the shape parameter α) and the recognition process that uses this shape model (the completely automatic determination of p and θ and the fitting parameter β) are addressed in detail in the following sections.

Fig. 1 Flowchart of our proposed method for recognizing the psoas major based on a model-building approach

(a) CT images

(b) Model-building process

(c) Recognition process

(d) Segmented muscle regions
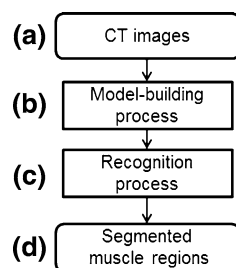
The validity of the shape model was evaluated by the segmentation result for the psoas major muscle by use of the Jaccard similarity coefficient $\left(\text{JSC} = \frac{A \cap B}{A \cup B}\right)$ [11] and the true segmentation coefficient $\left(\text{TSC} = \frac{A \cap B}{A}\right)$ [12]. A and B represent the muscle regions of the gold standard and the recognition result, respectively. The JSC describes the ratio of the area of intersection to the area of union. The TSC describes the fraction of the area of true detection to the area of the gold standard. The JSC is calculated for the 2D CSA and the 3D volume. It is calculated by the selected axial slice section at the Jacoby line from the top of the pelvis automatically. Then, we compare the thickness at the position at which radiologists measure the CSA for evaluation of our results. The method was implemented in a computer that included two 2.99-GHz CPUs with 16-GB memory.

2.3 Model-building process

The shape model of the psoas major muscle is constructed so that it can be applied to the recognition of the muscle for test cases. The anatomic definition of the psoas major muscle is shown in Fig. 2. Figure 2a shows the spindle-like shape of the psoas major, which is located symmetrically in the abdomen as indicated by arrows in Fig. 2b [14]. The radius of its transverse section is maximal at the longitudinal center and minimal at its origin and insertion. Including the psoas major muscle, all parts of the skeletal muscles are connected to the skeleton. The connection points are defined anatomically as origin and insertion. In this paper, these anatomic connection points are automatically detected as LMs for deciding the position of the muscle on the skeleton, which is generated by use of a previously reported method, described in [8]. Next, a line connecting these LMs is determined as a centerline for deciding the direction of the muscle. Finally, the surface of the muscle is approximated by a quadratic function, which is discussed in the following section.

In this way, the model for the muscle is described by a quadratic function that has two parameters: a shape parameter, α, which is defined by the training case and a fitting parameter, β, which is defined dynamically by the experimental case. The shape parameter describes the inherent shape of the psoas major muscle, and the fitting parameter describes the difference in shape between the model and a test case (i.e., individual variations).

Figure 3 presents a flowchart of the process of shape model generation. First, twenty cases in which there is no disease or muscular atrophy in the target region are selected. The first author of this paper manually extracted the muscle regions. These regions were then inspected, and, if necessary, the results were revised by the third author, who is a medical expert on anatomy. Next, the origin and insertion were inputted manually as fiducial points (referred as LMs). This process corresponds to the estimation of $\Pr(p \mid \text{vol})$ in expression (2).

Fig. 3 Flowchart of the shape model-building process

(a) CT images

(b) Manual extraction of muscle regions

(c) Input the anatomical feature points (LM)

(d) Anatomical centerline creation

(e) Approximation (quadratic curve)

(f) Shape model
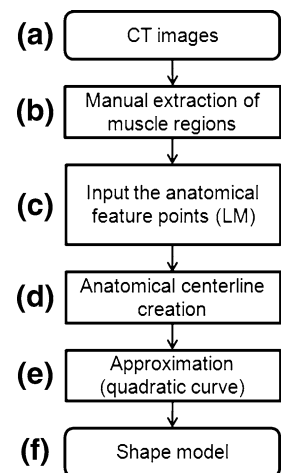
Fig. 2 Psoas major muscle (*flesh colored*, indicated by *arrows*). **a** Symmetrically located left and right psoas major muscles and **b** psoas major muscle in the intermediate part of a transverse section. The psoas major muscle is thin at the origin and insertion and thick in the middle

(a) Origin

lacuna musculorum

Insertion used in this method (Barycenter of lacuna musculorum)

Anatomical Insertion (lesser trochanter)

(b)
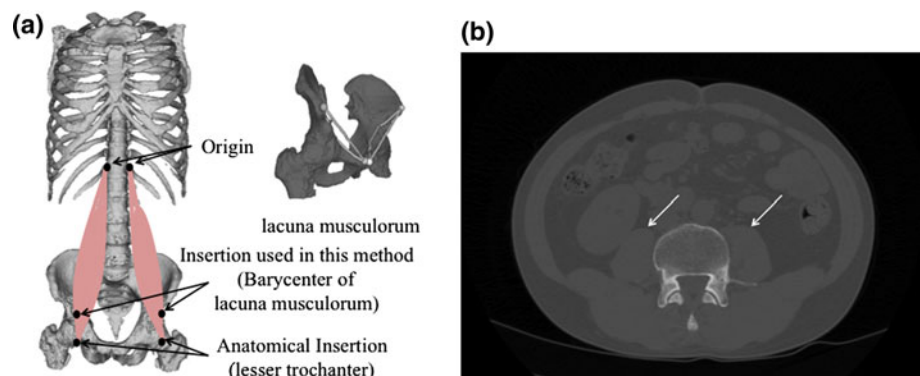
Table 1 shows the anatomic LMs of the origins and the corresponding insertion of the psoas major muscle. The psoas major muscle has five origins and one insertion. In this table, the insertion of the psoas major is defined as the center of mass of the lacuna musculorum, which is a point that the psoas major passes through. The LM of this insertion is therefore different from its anatomic definition. The aim of making this change is to assume a location that is always included in CT images of the torso. It is thought that the lacuna musculorum, which is used in this paper, can be used instead of the actual anatomic insertion, which is the lesser trochanter of the femur, because the psoas major passes through the lacuna musculorum [14].

Following the manual identification of origin and insertion, the anatomic centerline of the muscle is obtained by connecting the pair of LMs that were already inputted manually [corresponding to the determination of θ in expression (2)]. These anatomic centerlines describe the direction in which the muscle fiber runs. In the proposed technique, we then ascertain the overall direction from two or more centerlines. The straight line between the origin and the insertion can be used for recognizing the muscle orientation; the psoas major has five centerlines. Finally, we approximate its outer boundary to complete the shape model [corresponding to the determination of s in expression (2)].

The shape model of the psoas major is defined by a function that indicates the distance from the center of the muscle (centerline) to its outer border (indicated by the white curve in Fig. 4a and also indicated by arrows in b). A total of five shape model functions are generated by the pairs of corresponding origins and insertions. Each function is defined so that its centerline connecting the origin LM and insertion LM by the straight line is considered as the x-axis. The origin of the x-axis is defined as the point halfway between the anatomic origin point (i.e., the vertebra) and the insertion point (i.e., the center of the lacuna musculorum) of the psoas major muscle. The orthogonal direction becomes the y-axis. The values of y can be determined by substituting x values with a fixed interval to the functions in Table 2. In the recognition process, which is described later, this value of y is used as the structural element's radius for mask generation.

In the building of the model function, first, a Euclidean distance transformation [15] is applied to the muscle region obtained by manual extraction, and the distance value, y_i that corresponds to the x_i on each centerline voxel is obtained. Note that x_i and y_i are the coordinates for a set of points on the surface of the muscle region. Next, these distributions of the distance values are approximated by use of the following quadratic function:

$$y_i = \alpha_i x_i^2 + \beta_i (i = 1, \ldots, 5), \qquad (3)$$

where, i denotes the centerline corresponding to the origin and the insertion pair that constitute the LMs. α_i is the gradient and represents the peculiar outer shape of the psoas major, which is referred to as the outer shape parameter. β_i is the intercept of the function and indicates the maximum radius of the psoas major. This fitting parameter β_i that is appropriate for each test case is determined automatically in the recognition process. The value of x_i indicates the distance along the centerline from the midpoint and is used in the recognition process. The approximation accuracy of the quadratic function compared with the manual muscle shape is described as the R^2 value. The R^2 value is obtained as the square of the value, the covariance of the manual data point and the corresponding values on the approximated curve divided by the
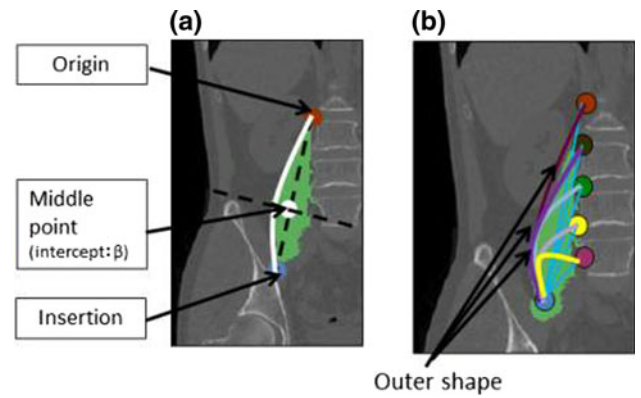
Fig. 4 Diagram of the shape model for the psoas major muscle (*solid line*). **a** Example of shape model for LM pair of thoracic vertebra XII and insertion (x-axis and orthogonal y-axis are indicated by *dotted lines*) and **b** five shape models of five LM pairs

Table 1 Correspondence between origin and insertion

Origin	Insertion
Thoracic vertebra XII	
Lumbar vertebra I	
Lumbar vertebra II	Barycenter of the lacuna musculorum
Lumbar vertebra III	
Lumbar vertebra IV	

Table 2 Functions with R^2 values in the outer shape model for the psoas major muscle

Origin	Approximate functions	R^2 value
Thoracic vertebra XII	$y_1 = -1.81 \times 10^{-4} x_1^2 + \beta_1$	0.753
Lumbar vertebra I	$y_2 = -4.29 \times 10^{-4} x_2^2 + \beta_2$	0.902
Lumbar vertebra II	$y_3 = -5.68 \times 10^{-4} x_3^2 + \beta_3$	0.855
Lumbar vertebra III	$y_4 = -8.01 \times 10^{-4} x_4^2 + \beta_4$	0.765
Lumbar vertebra IV	$y_5 = -9.20 \times 10^{-4} x_5^2 + \beta_5$	0.660

multiple of standard deviation of each. Table 2 lists the outer shape model functions generated by a quadratic curve approximation and the corresponding R^2 values; it indicates that the average R^2 value is 0.787, its maximum value is 0.902, and its minimum value is 0.660.

2.4 Recognition process

Figure 5 is a flowchart of the recognition process. The recognition process that uses the shape model generated as described above is conducted as follows. First, original CT images are inputted, and the segmented skeletal images are generated as mentioned above. Next, LMs, which are the anatomic feature points, are automatically recognized from these segmented skeletal images [corresponding to the determination of p in expression (2)]. Next, the anatomic centerlines are generated [corresponding to the determination of θ in expression (2)], and the shape model fitting process takes place [corresponding to the estimation of the fitting parameter β_i, a sub-parameter of s in expression (2)] in order that the psoas major muscle is recognized. Each model curve is fitted on the centerline based on the LMs. This curve gives the radius of the outer shape searching

area. Finally, the initial muscle region is determined with the use of this searching area, and then the region-growing technique [16] is applied for segmenting the final muscle region.

2.4.1 LM recognition

Each LM is placed on a muscle's origin or insertion, and its location corresponds to the manually extracted LM that was used in the model construction process. In the recognition process, LMs are set up in a completely automatic manner with the use of spatial positioning information on the segmented skeletal images. Each LM is determined in 3D space. First, we select the skeleton (Th12 and L1–L4) from the segmented skeletal images in which the LMs will be placed. Next, we determine the 2D axial plane from the selected skeleton. Finally, we determine target points in this 2D axial plane. The details are as follows.

The LM of the origin is determined by use of positional information from five points on the skeleton from the twelfth thoracic vertebra to the fourth lumbar vertebra. In the beginning of the process, the z coordinate of the LM (in the direction of the body axis) is determined at the slice through the center of gravity of each vertebra (Fig. 6a). Each vertebra is selected from the segmented skeletal images as mentioned above. Subsequently, the x and y coordinates of the LMs are determined. First, the line of symmetry that divides the human body area into two is obtained by use of the center of gravity in the human body area in the axial section (dotted line in Fig. 6b). Here, potential rotation of the body is incorporated because this method uses the positional information obtained from the skeleton, and the movement of the attached muscle is based on the skeleton. The positions indicated by the white points in Fig. 6b are automatically recognized in the area enclosed by the solid lines, with the following rules: they must be (1) on the surface of a vertebra, and (2) in the most

Fig. 5 Flowchart of the recognition process for muscle regions

(a) CT images

(b) LM recognition

(c) Centerline creation

(d) Model curve-fitting

Segmented muscle regions
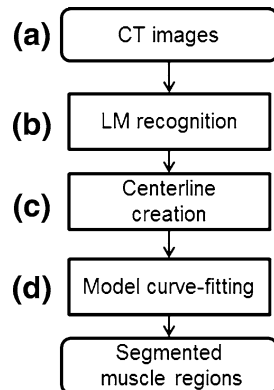
Fig. 6 Diagrams showing the anatomic feature point recognition. **a** Slice decision (*dotted line*) using position information for upper and lower skeleton. **b** Anatomic feature point recognition. The *dashed line* shows the line of symmetry; the *solid line* shows the area that was searched, and the *white dots* show recognized points
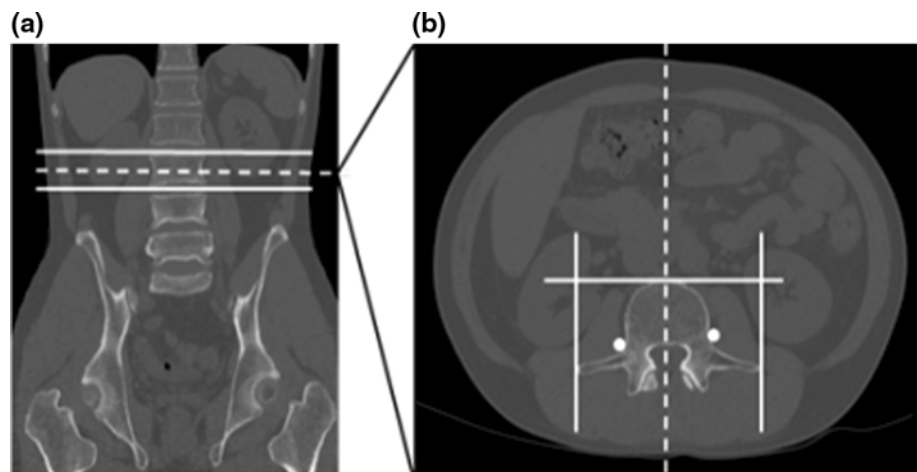
dorsal and (3) the most internal position of the selected skeleton. By this rule, the white point is located diagonally opposite the intersection of the solid lines; at the anterior of the vertebra and to the left and right edges of the vertebra in Fig. 6b. The lacuna musculorum is automatically recognized based on our previous work [17], and the center of gravity of the lacuna musculorum is determined as the LM of the insertion.

In this study, all of the LMs were correctly recognized because we employed all cases in which segmentation of the skeletons succeeded [8].

2.4.2 Centerline building

In the centerline-building process, we automatically connected the LMs that were determined above. The origins and their corresponding insertions specified in Table 1 are connected by the shortest possible straight lines, and five centerlines are generated symmetrically with respect to the spine. Figure 7 shows a volume rendering of a skeleton with anatomic centerlines.

2.4.3 Model curve fitting

In the shape model-fitting process, an appropriate fitting parameter β_i of each shape model y_i ($i = 1,\ldots,5$) is obtained from the input image by use of the model function of Table 2. β_i is obviously uniquely determined by the coordinate pair of x and y based on the function in Table 2. By defining the origin LM as $L_{oi}(u_i, v_i, w_i)$ and the insertion LM as $L_i(u, v, w)$ in correspondence with the centerline i, the values (x, y) obtained in the following expression are substituted for each function of Table 2:
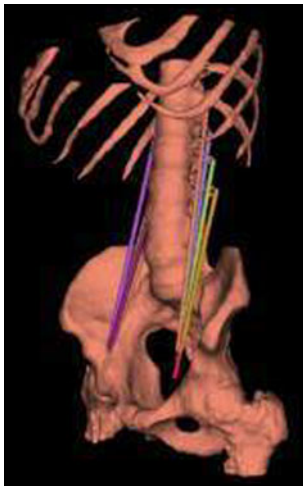
$$(x,y) = \left(\left| \sqrt{\left(u_i - \left(\frac{u_i + u}{2}\right)\right)^2 + \left(v_i - \left(\frac{v_i + v}{2}\right)\right)^2} \right|, 0 \right). \tag{4}$$

Expression (4) is used for calculation of β_i in expression (3). As already mentioned, the parameter α_i in expression (3) is determined in the model-building process as in Table 2. In Table 2, each β_i has not yet been decided on. β_i determines the vertex of the quadratic function, representing the thickness of the psoas major muscle. At the same time, β_i and LMs take into account individual differences in body size. β_i is obtained by substitution of the coordinate (x, y) in expression (3). In this study, we substituted the values for one LM point. At the LM point, y is zero and x is half the distance between two LM points. As a result, the shape model function that is appropriate for a specific test case is generated.

In the next step, the model functions generated above are used for segmenting of the muscle region. These five functions output the thickness of the psoas major muscle in each position by substituting the coordinate on the corresponding centerline. This coordinate is given by the distance along the centerline from the midpoint. All coordinates on the centerline are substituted for x_i in each function for determining the radius of the cross section in each axial slice. The calculated radius is used for generating a mask image. The 3D mask image is created by combining the sphere's structural elements with the various radii determined above. Sphere regions were created along the centerline; these were overlapped mutually, representing the shape of the muscle as a whole. The region defined by this shape model is employed as a mask image (Fig. 8a), from which the initial muscle candidate region is obtained by application of the Otsu threshold method [18] in this mask region.

This initial region is typically smaller than the true muscle region. Therefore, we made a fine adjustment on this initial muscle region by searching for similar pixel

Fig. 7 Volume rendering of skeleton with anatomic centerlines. *Each color* indicates a different anatomic centerline. Five centerlines are on each side of the psoas major muscle
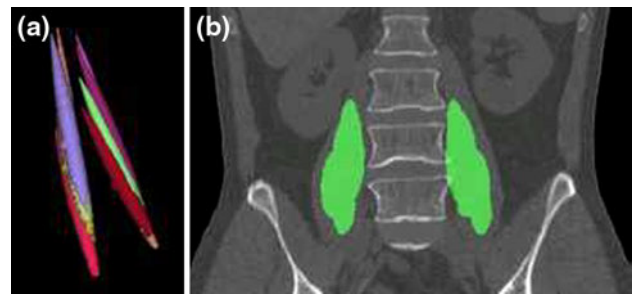
Fig. 8 Shape model of the psoas major muscle. **a** Psoas major muscle mask generated by the shape model function. The *different colors* correspond to the masks for five anatomic centerlines. **b** Example of mask image (*green*) on an original CT coronal image

values in a radial direction to obtain the definitive muscle region. The pixel values that are equivalent to the mean pixel value of the initial candidate region were sought radially at the boundary of the region and of the extended peripheral regions. This fine adjustment based on region-growing [16] is started from the axial section at the mid-point (Fig. 4a) in the mask region. The region-growing is controlled by the stopping rule that the area of the muscle cross section is smaller than the initial area in the middle section, i.e., keeping its spindle shape. Figure 8a shows a mask image generated by the shape model function. Each color represents the mask corresponding to each anatomic centerline. Figure 8b is the mask superimposed on the original CT image, showing that the initial mask region is smaller than the actual muscle region.

3 Results

We applied this scheme to 80 CT images. Table 3 lists the results of the recognition process in terms of the JSC and TSC for the entire volume of the recognition results. The average JSC and TSC were 0.723 and 0.762, respectively. Note that the patient with the large error had no disease in the muscle, but had a spinal curvature. This spinal curvature caused the imbalance between the right and left muscles in the body compared to the normal cases, which caused the difference in the muscle volumes between the right and left sides. As a result, the extracted region on one side is expanded and that on the other side is contracted, resulting in over- and under-recognition, respectively.

Figure 9 shows the JSC of the CSA in each vertebral body. As shown in the figure, a high accuracy rate of about 90% was obtained in each vertebral body section from L1 to L4. Figure 10 shows the recognition results for the psoas major. The green, blue, and red regions indicate the region of overlap between the gold standard and the recognition results, the area of overextraction, and the area of under-extraction, respectively. Figure 10a is a 3D view, which represents the need for improvement in the accuracy around the origin of the psoas major. The region near the Th12 section has a low recognition accuracy compared to

that in the other sections, as shown in Fig. 9. Moreover, the JSC value in the L3 section is lower than those in the L2 and L4 sections. This is a result of the overextraction of the blood vessel, which is confirmed by the blue area in Fig. 10a. The high JSC values in the L4 and L5 sections, accordingly, indicate that the proposed method is effective for automatic measurement of the volume of the psoas major near the Jacoby line, which is where clinical radiologists measure a muscle's CSA and thickness. An enlarged view of the result in this cross section is shown in Fig. 10b.
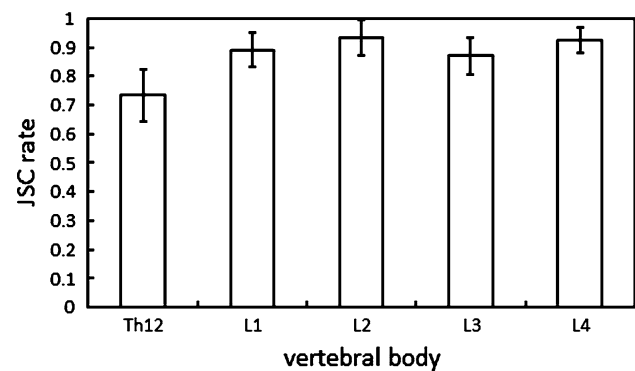
Fig. 9 Average JSC of CSA in each vertebral body for 80 cases. Each *error bar* indicates the maximum and the minimum JSCs
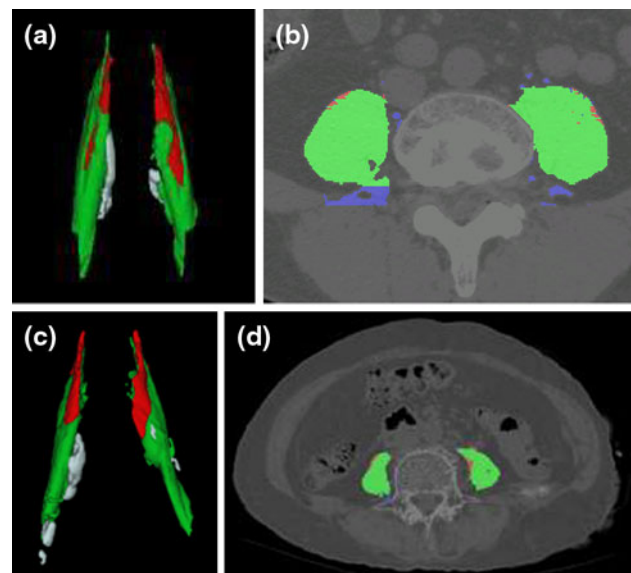
Fig. 10 Segmentation results for psoas major muscle compared to the gold standard, for a 49-year-old male (**a**, **b**) and an 84-year-old female (**c**, **d**). **a**, **c** 3D view of segmentation results. **b**, **d** Segmentation results compared to the gold standard in transverse section at the Jacoby line. *Green* indicates the area of overlap; *blue*, the area of overextraction; and *red*, the area of underextraction

Table 3 Recognition accuracy for the psoas major muscle

	JSC	TSC
Min.	0.683	0.677
Max.	0.904	0.971
Average	0.723	0.762

JSC Jaccard similarity coefficient, *TSC* true segmentation coefficient

4 Discussion

As mentioned above, our method was not intended for measuring the muscles in patients with severe muscle diseases. Rather, the model created with normal cases can be used for recognizing cases with abnormal muscles. Our database did not contain cases with muscle disease, because CT images were not intended for diagnosis of muscle diseases. However, we also tested the proposed method in some aging patients. Elderly patients often have a bent spine or decreased muscle [3]. Figure 10c shows the segmentation results for an 84-year-old woman. This woman had a slight curvature of the spine. Accordingly, the psoas major muscle had decreased in size on one side. Figure 10c visually confirms the decrease of the muscle on the left side. The JSC and TSC for this case were 0.772 and 0.848, respectively.

Figure 10d shows the results in the transverse section at the Jacoby line. The results indicate that the segmentation performance for aging patients is also acceptable at the Jacoby line. The root mean square error for the muscular thickness was 3.44 mm (5.50 pixels), which indicates that our technique is also effective for the automatic quantitative measurement of the thickness of the psoas major muscle.

Regarding the proposed method, the anatomic shape of the psoas major muscle could be reproduced through the use of a mathematically simple quadratic function with two parameters that approximated the muscle shape, according to the mask area superimposed upon the original CT image in Fig. 8b. The evaluation of the accuracy of the model function for the psoas major muscle shape in terms of the R^2 value is shown in Table 2. The average R^2 value was 0.787, and the value for the function y_5 was low compared with those for the function y_1–y_4. The reason is that the region of the psoas major is small in the vicinity of L4, where the end point of the psoas major converges, compared with the other areas. It is therefore difficult to construct a precise model from a simple function like the quadratic function proposed in this study. Such a function is suitable; however, for the approximation of a round shape with use of few parameters. It would be necessary to verify in the future whether the shape of a muscle can be expressed by use of other functions.

As mentioned above, in this research, the shape of the psoas major muscle was modeled by a mathematical function, which was then used for muscle recognition in a CT image. As a result, we were able to show not only that skeletal muscle recognition in a CT image was possible, an achievement that a past study considered difficult, but also that this method could be applied to images obtained by other imaging modalities because it is based on anatomic information, as in an MRI, for example.

We should note that the technique of the proposed method depends on the segmentation results for the skeleton [8]. Moreover, it is also possible to correct LMs that have been placed at wrong positions, if the necessity arises, by manual intervention. Further, such semiautomatic correction is inexpensive in terms of time as compared to the manual segmentation of an entire muscle region in the original CT images.

The processing time required for the proposed technique is about 3 min. This reduces the muscle measurement workload of the radiologist considerably. For instance, when the authors (N.K., a researcher in engineering who manually segmented the data, and H.C., a specialist in anatomy who verified the accuracy based on medical knowledge) completely segmented a muscle manually, 30 min or more time was needed. By semiautomatic extraction with the proposed technique, it was possible to complete the segmentation in about 10 min. In this regard, with the proposed automated method, a reduced workload becomes possible in clinical settings for radiologists who currently measure the muscular thickness and volume manually.

5 Conclusion

A fully automated method for recognizing the psoas major muscle in X-ray CT images, by use of a shape model, is proposed in this study. Two parameters—an outer shape parameter and a fitting parameter—are used for the definition of a quadratic function that approximates the shape of the muscle, in this case the spindle shape of the psoas major. This method was applied to 80 CT cases. In the recognition of the psoas major, the average values for the JSC and the TSC were 0.723 and 0.762, respectively. These results show that the shape model can provide the initial region for distinguishing the skeletal muscle from other organs, which is otherwise difficult to do in CT images.

The mean error for the thickness was 3.4 mm in the section of the Jacoby line. In addition, the required measuring time was reduced by 90% as compared to manual extraction and by 65% if semiautomatic correction was included. This result shows that the proposed method can greatly reduce the time required for certain tasks performed by radiologists. Therefore, the proposed method can be used for the analysis of CSA and muscular thickness in a transverse section, offering radiologists an alternative to manual measurement.

We considered that the error margin in a 2D section was within the clinically allowable range according to the anatomic specialist. Currently, the muscular volume is not evaluated quantitatively in clinical situations. However,

quantitative 3D analysis of the muscle volume would become possible by the proposed method with minimal manual correction by a radiologist. We applied the model only to subjects with normal muscles as a preliminary study. In the future, the method should be applied to cases with muscle atrophy for verifying the possibility of estimating changes in muscle thickness.

References

1. Cabinet Office. Annual Report on the Aging Society 2006, Available: http://www8.cao.go.jp/kourei/english/annualreport/2006/06wp-e.html.

2. Sturnieks DL, George R, Lord SR. Balance disorders in the elderly. Neurophysiol Clin. 2008;38:467–78.

3. Takahashi K, Takahashi HE, Nakadaira H, Yamamoto M. Different changes of quantity due to aging in the psoas major and quadriceps femoris muscles in women. J Musculoskelet Neuronal Interact. 2006;6:201–5.

4. Hohne KH, Pflesser B, Pommert A, Riemer M, Schubert R, Schiemann T, Tiede U, Schumacher U. A realistic model of human structure from the visible human data. Methods Inf Med. 2001;40:83–9.

5. Qin Y, Cheng Z, Zhuang T, Wang H, Wang Y, Yan Z, Tiede RM, Hohne U. Interactive segmentation of muscles and 3D representation of meridians based on visible human. Conf Proc IEEE Eng Med Biol Soc. 2005;5:5116–9.

6. Gilles B, Moccozet L, Thalmann NM. Anatomical modelling of the musculoskeletal system from MRI. Med Image Comput Comput Assist Interv. 2006;9:289–96.

7. Ng HP, Hu QM, Ong SH, Foong KWC, Goh PS, Liu J, Nowinski L. Segmentation of the temporalis muscle from MR data. Int J Comput Assist Radiol Surg. 2007;2:19–30.

8. Zhou X, Hayashi T, Han M, Chen H, Hara T, Fujita H, Yokoyama R, Kanematsu M, Hoshi H. Automated segmentation and recognition of the bone structure in non-contrast torso CT images using implicit anatomical knowledge. Proc SPIE, 2009;7259, 72593S. doi: 10.1117/12.812945.

9. Zhou X, Hayashi T, Hara T, Fujita H, Yokoyama R, Kiryu T, Hoshi H. Automatic segmentation and recognition of anatomical lung structures from high-resolution chest CT images. Comput Med Imaging Graph. 2006;30(5):299–313.

10. Zhou X, Kamiya N, Hara T, Fujita H, Chen H, Yokoyama R, Hoshi H. Automated segmentation and recognition of abdominal wall muscles in X-ray torso CT images and its application in abdominal CAD. Int J Comput Assist Radiol Surg. 2007;2: 389–90.

11. Anderberg MR. Cluster analysis for applications. Academic press; 1973.

12. Hori D, Katsuragawa S, Murakami R, Hirai T. Semi-automated segmentation of glioblastoma multiforme on brain MR images for radiotherapy planning. Jpn J Radiol Technol. 2010;66(4):353–62.

13. Kernan WN, Viscoli CM, Makuch RW, Brass LM, Horwitz Rl. Stratified randomization for clinical trials. J Clin Epidemiol. 1999;52:19–26.

14. Drake R, Vogl W, Mitchell AWM. Gray's anatomy for students. Churchill Livingstone; 2005.

15. Saito T, Toriwaki J. New algorithms for Euclidean distance transformation of an n-dimensional digitized picture with applications. Pattern Recognit. 1994;27(11):1551–65.

16. Gonzalez RC, Woods RE. Digital image processing, 2nd ed. Prentice Hall; 2002.

17. Kojima S, Zhou X, Hara T, Fujita H, Azuma K, Yokoyama R, Hoshi H. Automated analysis of bone structures for anatomical structure recognitions on torso X-ray CT images. IEICE Tech Report (in Japanese). 2006;106(343):43–8.

18. Otsu N. A threshold selection method from gray-level histograms. IEEE Syst Man Cybern. 1979;9(1):62–6.